

Experimental Verification of a High-Current Cathode Thermal Model*

K. D. Goodfellow[†] and J. E. Polk[†]
*Jet Propulsion Laboratory
California Institute of Technology
Pasadena, California*

Abstract

A series of models have been developed to describe the temperature distribution of thermionic cathodes in high current discharges in an effort to evaluate cathode service life. A number of experimental measurements have been made to validate these models and provide values of the input parameters. A database of axial temperature distributions on a cylindrical, 2 percent thoriated tungsten cathode has been collected for a current level of 1000 A for argon mass flow rates of 0.060 to 0.878 g/s and ambient gas pressures ranging from 1.5 to 6.0 kPa. The changes in the flow rate were found to have no significant effect on the axial cathode temperatures. Electron temperature measurements were made utilizing the method of relative line intensity ratios. The radial temperature profiles are flat for the low pressure case and increase radially for the high pressure cases. The variation of the attachment area with current and pressure was characterized by measuring the intensity distribution of an argon ion line near the cathode surface. For all of the pressures considered the arc is attached in an annular ring on the cathode tip and not on the centerline. Materials analysis of the cathode following a test at 1000 A and 6.0 kPa for two hours revealed that the thorium tends to accumulate at the tip, is depleted on the shaft, and a transition occurs in between. A minimum in the work function therefore occurs in an annulus around the cathode tip. Model comparisons with the data show excellent agreement for all of the parameters.

Introduction

The service life of thermionic cathodes is important for a number of high current discharge devices, particularly several classes of electric thrusters such as electrothermal arcjets and magnetoplasmadynamic (MPD) engines. Low thrust levels dictate burn times of several thousand hours, and the cathodes of these devices are often the life-limiting component. High-current cathodes are subject to failure modes which can be classified as either event-consequent or the result of damage accumulation. Event-consequent failures, such as cathode melting as a result of excessive resistive heating, are the result of a single catastrophic event and can be adequately characterized by testing alone. However, it is impractical to characterize the failure risk associated with damage accumulation failure modes by testing alone because of the extremely long test durations required to observe the failures. Validation of cathode service life under conditions where damage

Copyright © 1995 American Institute of Aeronautics and Astronautics, Inc., all rights reserved.
Member of the Technical Staff, Advanced Propulsion Technology Group

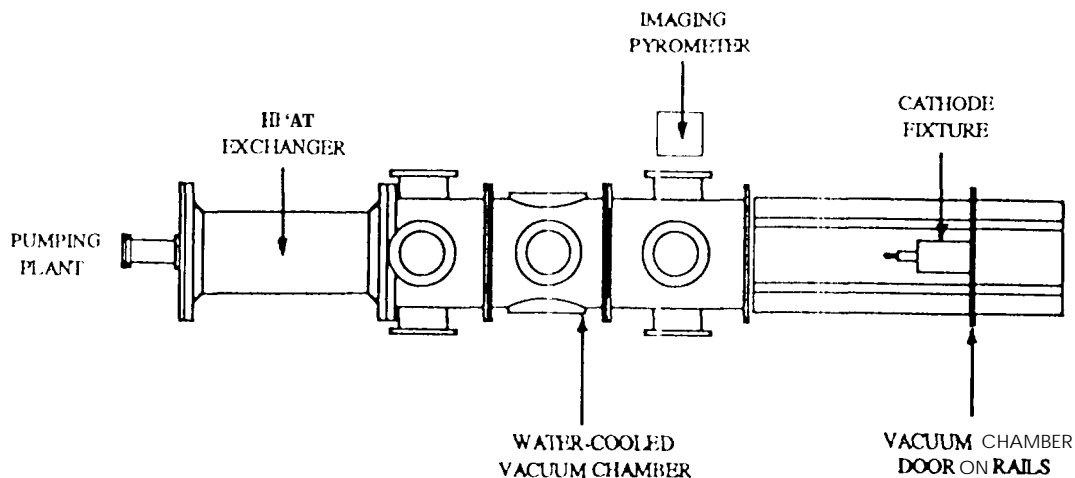


Figure 1: Diagram of the cathode test facility.

cooled copper liner has been inserted in the middle two segments to permit long-duration operation. As the schematic in Fig. (2) shows, the first segment forms the discharge chamber. A water-cooled, ring-shaped copper anode with a diameter of 7.6 cm is mounted on a flange located between and electrically isolated from the first two tank segments. The cathode fixture mounted on the vacuum chamber door is composed of two coaxial tubes electrically isolated from each other and the door with mica rings. The inner tube serves as the cathode current feed and has a water-cooled cap on the end to which the cathode is clamped. The outer tube is electrically floating and has a water-cooled copper disk mounted on the end with an aperture through which the cathode protrudes. The propellant gas is injected between the two tubes and flows into the discharge chamber through an annulus around the base of the cathode. The interelectrode gap is set by the thickness of a spacer in the cathode assembly. The cathodes used in this investigation were rods of 2 percent thoriated tungsten 76 mm long and 9.5 mm in diameter with hemispherical tips. The last tank segment contains a heat exchanger made of water-cooled, finned copper tubing to cool the exhaust before it enters the pumping system. The tank has a number of ports which provide optical access to the discharge chamber as well as the plume. In addition, the cathode and the discharge can be viewed along the tank axis through a window at the rear of the tank.

The vacuum chamber is pumped by a 610 l/s Roots blower backed by a 140 l/s Stokes mechanical pump. The system is capable of achieving a vacuum of less than 0.13 Pa with no propellant flow and approximately 80 Pa with an argon flow rate of 0.75 g/s. Higher ambient gas pressures are achieved by throttling the pumping speed with a valve on a bypass around the main vacuum valve. The ambient pressure can be controlled to within approximately ± 30 Pa. The arc is powered by two Miller welding power supplies, each of which can provide 1000 A at a load voltage of 40 V continuously or 2000 A at 40 V with a 50 percent duty cycle. The initial arc breakdown is accomplished with a 4 A, 850 V start supply.

accumulation failure modes are critical therefore must rely heavily on modeling of the physics of failure. The role of testing is to identify the critical failure modes, validate the models of failure and provide information on the model input parameters such as material properties and operating environment.

High current cathodes are being studied at the Jet Propulsion Laboratory as part of the Advanced Propulsion Concepts program. The goal of the program is to develop long-lived cathodes and the analytical tools to validate their service life. Cathode erosion, which appears to be the dominant damage accumulation failure mode, has been shown to depend strongly on the cathode temperature [1]. Therefore, part of this study is intended to provide a simple means of predicting the cathode temperature for various thruster operating conditions. In addition, the thermal characteristics of the electrodes must be known to compute the overall thruster thermal loads to the spacecraft. Models must also provide the appropriate boundary conditions at the cathode surface for models of the operating characteristics of the thruster. For example, the current contours within the magnetoplasmadynamic thruster cannot be specified independently of the cathode temperature distribution because the majority of the current is from thermionic emission. Since the cathode model boundary conditions also depend on the characteristics of the main plasma, the two models must be ultimately coupled to obtain an overall model of the cathode region of the thruster.

A series of models describing the cathode and plasma interaction are being developed. The cathode model consists of two parts, namely a near-cathode plasma model and a thermal model of the cathode [2,3,4]. The near-cathode plasma model connects the properties of the main plasma with the cathode. Specifically, given the plasma properties within a mean-free-path of the surface, the near-cathode model predicts the heat flux and current density to the cathode surface. With these boundary conditions and the traditional thermal transport mechanisms, the thermal model can predict the temperature distribution within the cathode. Because of the interdependency of the two models, they must be solved simultaneously. The input parameters used by the model for the plasma consist of the sheath voltage, the pressure, the ionization energy of the gas, the ion mass, the surface work function, and the surface temperature. The arc attachment area is also specified to limit the total current, which is calculated using the given attachment area and the calculated current density distribution. The thermal model inputs consist of the base temperature or heat flux, the convection coefficient and environmental temperature, the surface emittance and environmental temperature, and the material thermal conductivity and resistivity. A series of thermal models have been developed with different levels of approximation. The nonlinearities of the system equations can present numerical difficulties. The simpler, one-dimensional models can be used to provide starting points for the more complete two-dimensional models, significantly reducing the computational time required. Although the quasi-two dimensional models provide a good first approximation, a two-dimensional model is required for a detailed understanding of the processes involved.

The focus of the experimental part of the program is to test new cathode concepts, identify the critical failure mechanisms, provide a database of measurements to validate the cathode models, and determine the values of the critical model drivers such as work function and gas pressure. The purpose of this paper is to present a database of temperature profiles recently obtained over a range of ambient pressures and current levels for cylindrical, 2 percent thoriated tungsten cathodes. Comparisons of the model with preliminary thermal data showed good agreement at currents below about 1000 A and pressure levels greater than 1.5 kPa [3], so these experiments concentrated on this parameter range. In addition, the size of the attachment area and electron temperature were characterized to provide inputs to subsequent modeling efforts.

Experimental Apparatus

The Cathode Test Facility

The cathode test facility is shown in the diagram in Fig. (1). The stainless steel vacuum chamber is 0.5 m in diameter and 2.4 m long and is composed of 4 water-cooled cylindrical segments. In addition, a water-

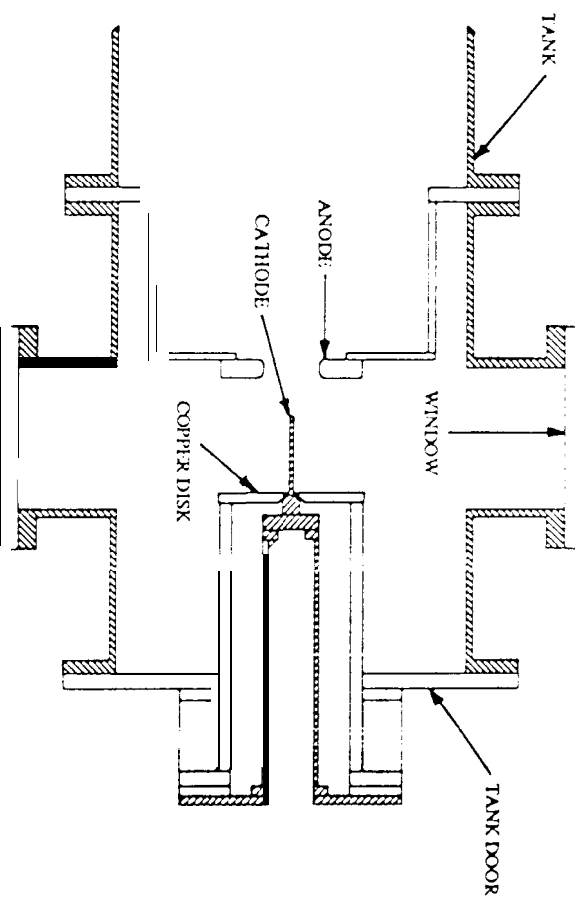


Figure 2: Schematic of the electrode configuration.

Diagnostics

The factory shunts in the Miller welders have been replaced with precision shunts that are used to monitor the arc current. The terminal voltage is measured at the current feedthroughs into the tank. The propellant flow rate is measured with a Sierra Instruments Side-Trak Model-830 flow meter and a Micromotion Model-D6 flow meter and controlled with a throttling valve located just upstream of the inlet to the cathode fixture. The flow meter output was calibrated by measuring the mass loss from an argon bottle as a function of time. Three MKS Baratron capacitance manometers with ranges of 0-133 Pa, $0-1.3 \times 10^4$ Pa, and $0-1.3 \times 10^5$ Pa are used to monitor pressures. The three transducers are mounted in a single manifold with two input tubes. One line measures the tank pressure through a feedthrough on the chamber door. A special cathode was fabricated with a 1 mm diameter hole bored the entire length along the centerline, which serves as a pressure tap to measure the pressure at the cathode tip. This pressure tap was connected to the other manifold inlet. Either pressure could be read independently by valving off the other input. These parameters and a number of facility temperatures are recorded with a Macintosh computer system utilizing LabView software and National Instruments multi-function I/O cards.

A CHDTVC 2250-1D (Charge Injection Device (CID) camera was chosen as an optical pyrometric sensor to measure the two dimensional temperature field on the cathode. The system optics are composed of two interference filters with a 10 nm bandpass centered at 632.8 nm and a long pass filter with a cutoff wavelength of 570 nm. The camera lens aperture is fixed at a relatively small value of $f/4$ and neutral density filters are used to control the image intensity. The imaging array has 512×512 CID detectors which are read out at a maximum rate of thirty times per second. These values are converted to an analog signal, which is then further processed and output as a normal video signal by the camera electronics. The video signal is digitized by a Data Translation DT-2862 8-bit frame-grabber board, which yields a final value between 0 and 255 corresponding to the incident power. The camera output was calibrated as a function of incident radiance using a tungsten ribbon lamp. The calibration procedure and a detailed error analysis for the temperature measurements are discussed in [5]. A surface emittance value of about 0.57 was used for all thermal data

analysis based on measurements made in Ref [5].

In the experiments the camera and optics were mounted outside the chamber about 39.5 cm from the cathode. The video output from the camera was digitized to provide real-time monitoring of the temperature distribution. One line in video memory chosen 10 correspond to the **axis** of the cathode was sampled from each frame. A given number of lines were averaged, displayed in **real** time, and periodically stored on disk.

The camera was also used to study the extent of the arc attachment region. Two interference filters with a 10 nm bandpass centered at 488 nm were used to select radiation from an intense argon ion line. Entire images of the cathode and near-cathode discharge region were then captured with the frame grabber board and analyzed to yield the lateral intensity distribution. These measurements were used to calculate an upper bound on the arc attachment area and the **average** current density in the attachment zone.

Emission spectroscopy was also used to determine the **electron** temperature near the cathode tip and downstream of the tip. The system was set up to form an image of the cathode on a screen with a lens mounted outside the vacuum chamber. A length of fiber optic cable was installed with the 100 micron diameter inlet located at the center of the screen and flush with the image plane. The screen and fiber inlet were mounted on a micrometer-operated X-Y translation stage so that the inlet could be positioned at any desired point in the image. With this technique, light-gathering with high spatial resolution from any image point could be achieved. The light emerging from the fiber exit was focused on the entrance slit of a one-meter McPherson monochromator using an optical system designed to match the fiber numerical aperture with that of the monochromator. Variable monochromator slits were set at 30 to 50 microns and a 1200 groove per mm grating was used to disperse the light, providing a potential resolution in first order of () 10 Angstroms. The output of a Hamamatsu R928 photomultiplier tube was filtered (30 Hz corner frequency with 12 dB/oct rolloff) and stored on a computer. The translation stage was moved vertically by a motorized stage and positioned axially manually. Scans were performed at several axial locations moving away from the cathode tip, and then some of these points were repeated moving back towards the tip. The vertical intensity scans were then Abel inverted to produce radial emittance profiles [(i) Additional filtering of the data was done within the Abel inversion routine using ii FIR Blackman windowed filter. For each case, two vertical scans were averaged and centered. The Abel inversion routine then folds the data set for a total of four averaged half-profiles, and performs the Abel inversion.

Experimental Results

Mass Flow Rate Effects

The focus of this experiment is the development of a database of temperature measurements for use in validating the models. The axial temperature distribution in the first 15 to 40 mm of the cathode (measured from the tip) was determined using the imaging pyrometer for current level of 1000 A, tank pressures of 1.5, 3.0, 4.5 and 6.0 kPa and an argon mass flow rates of 0.060 to 0.878 g/s. Typical results are shown in Figures (3) (6). Additional data are presented in Refs. [5] and [7]. The run numbers are included to show the order in which the experiments were performed. At lower pressures a temperature peak is located on the shaft of the cathode, while at higher pressures the peak is located on the tip. Many of the temperature profiles at higher pressure also show a change in slope near the tip. The intensity peak at the tip may contain some contribution from plasma radiation, either the continuum in the 10 nm bandpass of the 632 nm interference filter or the integrated effect of plasma radiation collected in the wings of the blocking filters. However, measurements of the plasma intensity off of the cathode surface indicate that this contribution is small. In addition) the timescale for decay of the tip intensity peak when the arc is extinguished is much longer than the plasma decay timescales, proving that the peak is due to surface luminosity.

The profiles in Fig (1) demonstrate the degree of irreproducibility in the cathode temperature for the same operating point. While the tip temperature is generally quite repeatable, temperatures on the shaft can vary by as much as 100 K from one trial to the next. The shapes of the curves are all very similar,

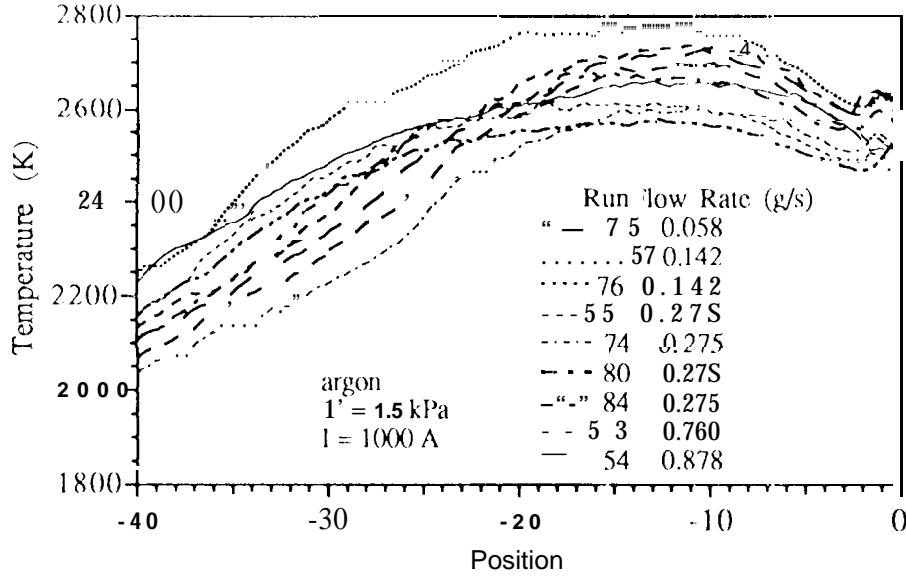


Figure 3: Axial temperature distribution for a tank pressure of 1.5 kPa

but in some cases they are displaced upward by the appearance of a temperature peak or plateau upstream of the tip. This suggests that additional heating is occurring in this location which pulls the distribution to higher temperatures. Some of the irreproducibility can be attributed to varying run durations, because the temperature distribution appears to evolve with time. No distinct affect of the mass flow rate on the temperature profiles could be found.

Electron Temperature Measurements

Electron temperature measurements have been made downstream of the cathode tip to help characterize the plasma for verifying the model predictions. A new cathode was installed for these tests. One method of determining the electron temperatures is using the method of relative line intensity ratios. The temperature is determined from the equation

$$kT_e = \frac{E_u - E_l}{\ln \left(\frac{\lambda_{st} A_{ul} g_u \epsilon_{st}}{\lambda_{mn} A_{lk} g_m \epsilon_{mn}} \right)} \quad (1)$$

where k is Boltzmann's constant, T_e is the electron temperature, E_s is the energy of level "s", λ_{st} is the wavelength for the transition between levels "s" and "t", A_{st} is the transition probability, ϵ_{st} is the measured emittance, and g_s is the degeneracy of level "s" [8]. For this study the ArII 401.4 and 410.4 nm lines were used. The resulting radial temperature distributions are shown in Figs. (7) through (10). The oscillations in some of the curves are likely a result of plume oscillations that were observed during the tests. The axial temperature distributions in Fig. (11) were obtained by curve fitting a line to the portion of the radial curves near the centerline. In general the temperatures decrease approximately exponentially with increasing distance from the cathode tip. The temperatures for 4.5 and 6.0 kPa begin to rise again around 4 mm from the tip. Also, the electron temperature decreases with increasing pressure, as expected. The temperature

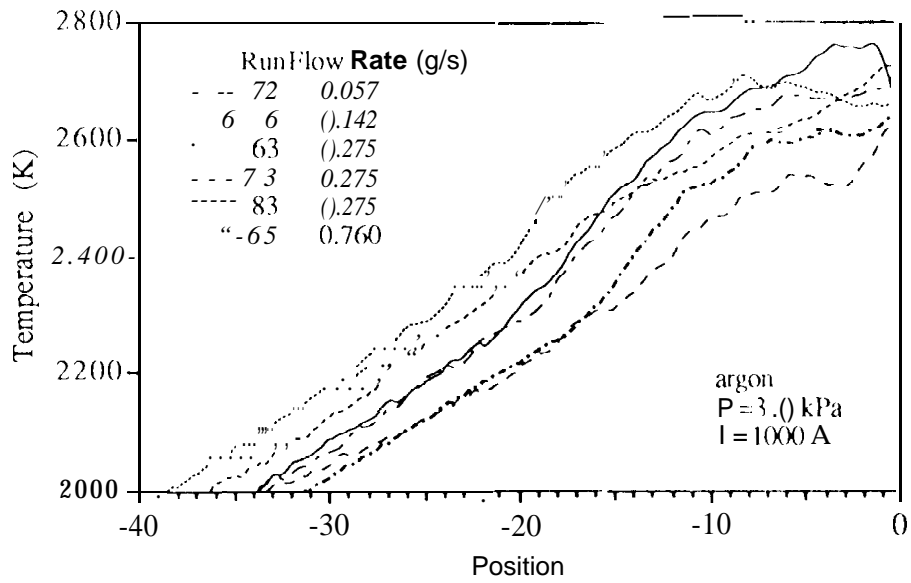


Figure 4 Axial temperature distribution for a tank pressure of 3.0 kPa

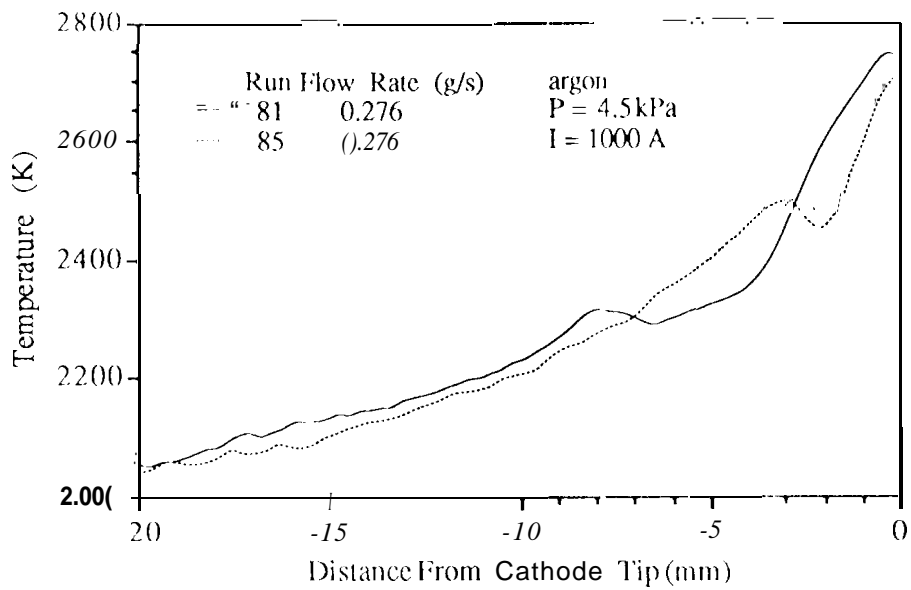


Figure 5: Axial temperature distribution for a tank pressure of 4.5 kPa.

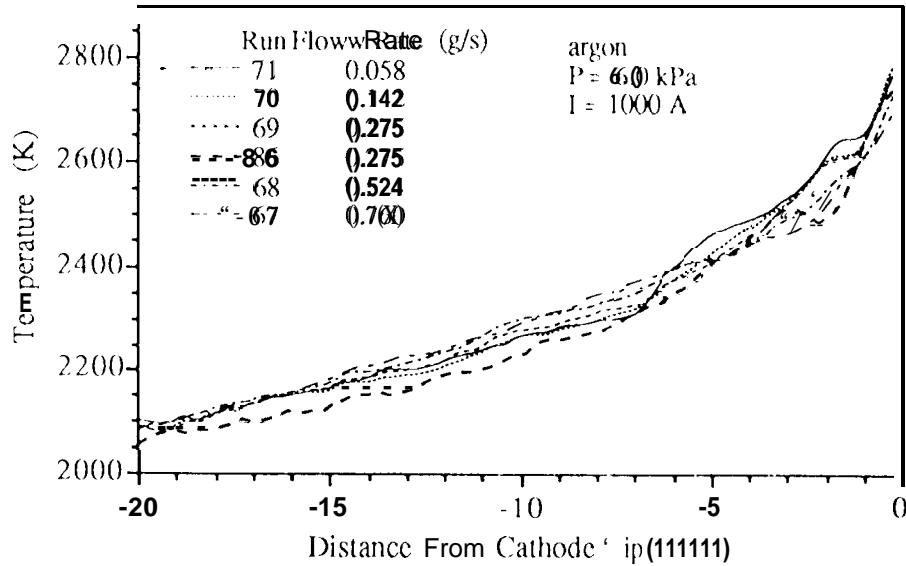


Figure 11: Axial temperature distribution for a tank pressure of 60 kPa.

profiles are flatter radially as the pressure is decreased. As the pressure is increased the electron temperatures begin to increase radially suggesting that the arc attachment is concentrated in an annulus near the edge of the cathode. Additional information discussed below will substantiate this idea. The data were less repeatable decreased at the higher pressures.

The electron temperature can also be calculated by plotting the logarithmic term of Eq. (2) versus the excited state energy.

$$\ln\left(\frac{N_n}{g_n}\right) = -\frac{E_n}{kT_e} + const. \quad (2)$$

This plot is shown in Fig. (12) for points located 0.254 mm and 2.79 mm downstream of the cathode tip. The ArII 397.9, 405.3, and 407.2 nm lines were used in addition to the 401.4 and 410.4 lines used previously. Clearly a single line will not fit the data correctly, indicating that nonequilibrium may be present. A line plotted through the three left points yields electron temperatures near those calculated using the line intensity ratio technique. Temperatures calculated using a line fit through the right three points yields a substantially lower temperatures (typically around 0.3 to 0.7 eV). It is unusual that the higher energy levels would have a lower temperature than the lower levels, indicating that this may be the result of an instrument error.

Filter photography has been used to determine the relative strengths of the argon 488 nm ion line. Contour plots of the Abel inverted images of the discharge region captured with the CHD camera using two 488 nm interference filters are shown in Fig. (13) through Fig. (16). The contours represent lines of constant camera response in gray levels and start from one on the outside, increasing inward in increments of one. A very interesting characteristic is observed in all of the cases. The largest gradients in the ion intensity are found near the corner of the cathode indicating that the majority of the arc attachment is in a thin annulus around the tip, and not on the centerline as with arcjet thruster cathodes. This current concentration moves towards the centerline as it moves away from the tip to form a conical current envelope. In addition, there is a depression in the intensity values in the center beginning about one millimeter from the the tip. That

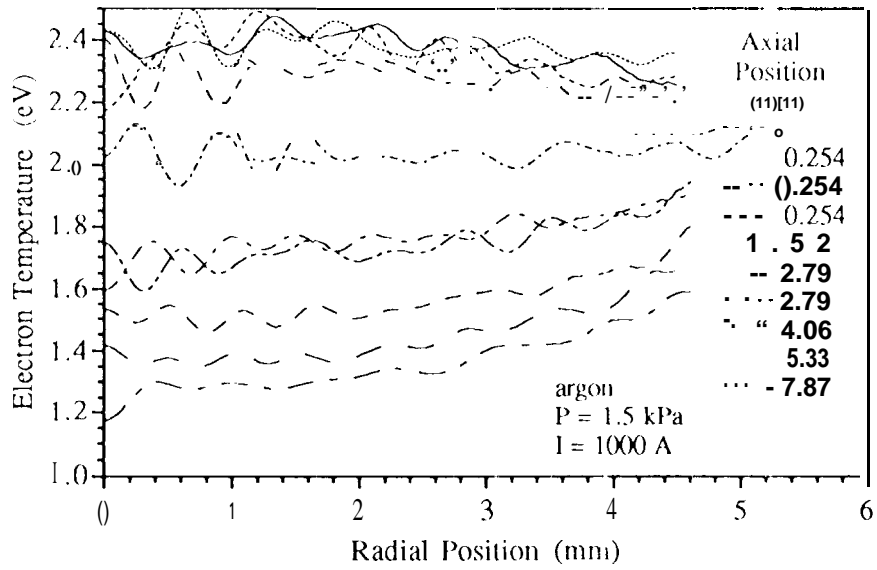


Figure 7: Electron temperature as a function of radius and axial position for a tank pressure of 1.5 kPa

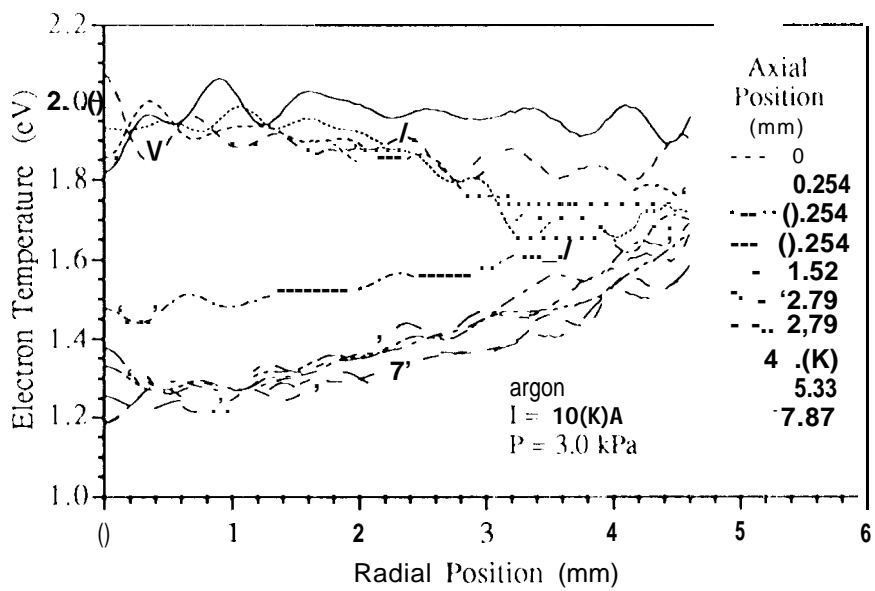


Figure 8: Electron temperature as a function of radius and axial position for a tank pressure of 3.0 kPa

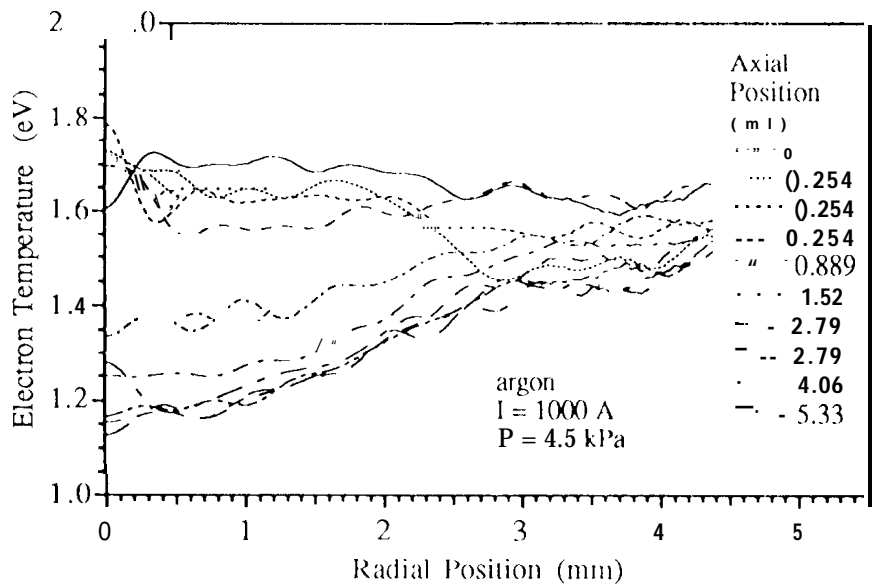


Figure 9: Electron temperature as a function of radius and axial position for a tank pressure of 4.5 kPa

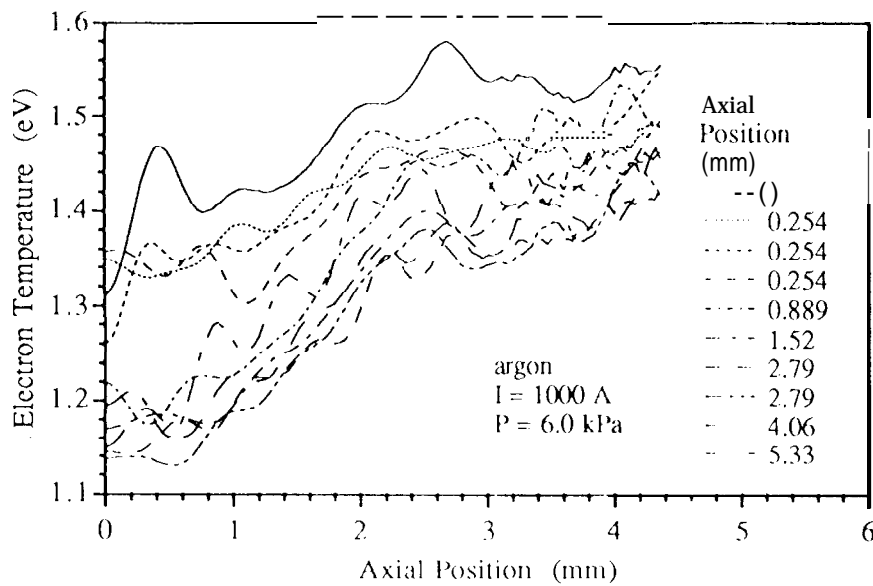


Figure 10: Electron temperature as a function of radius and axial position for a tank pressure of 6.0 kPa

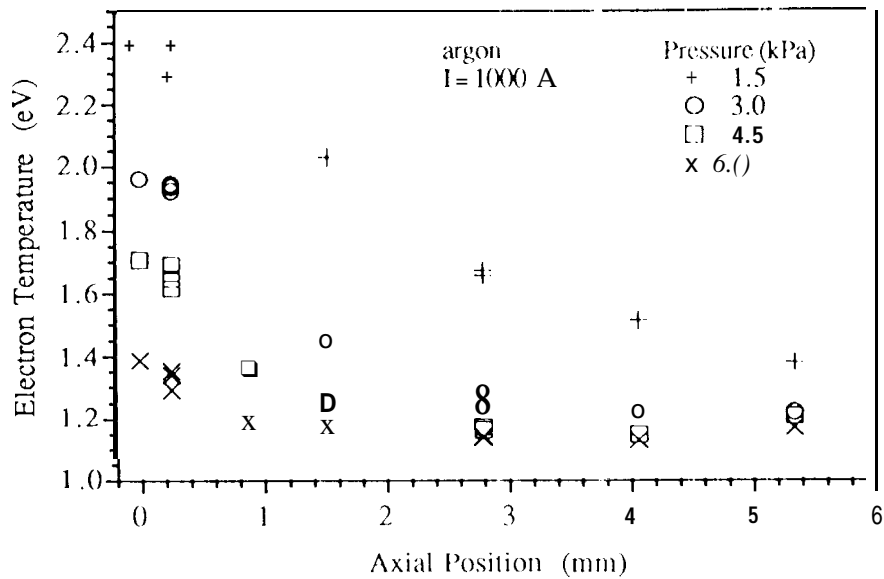


Figure 11: Centerline electron temperature as a function of axial position

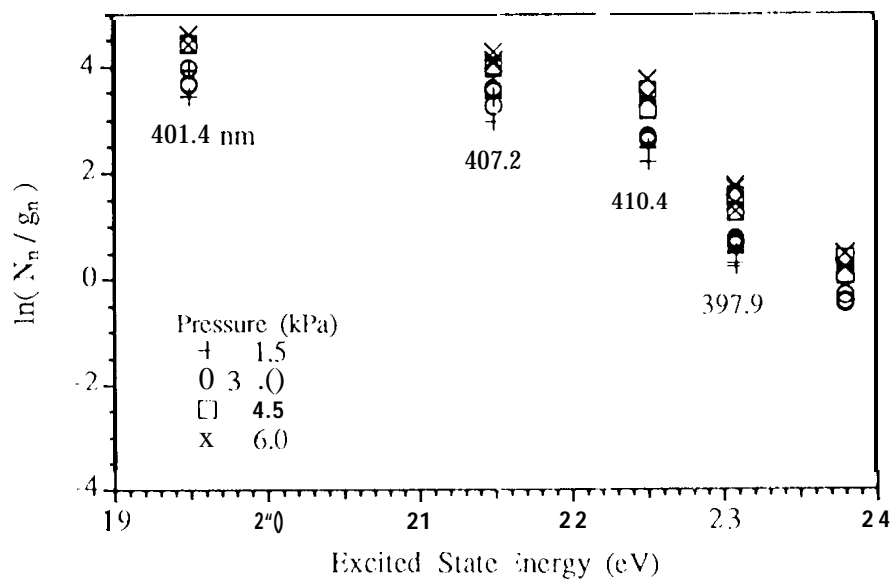


Figure 2: Boltzmann fit to electron temperature data.

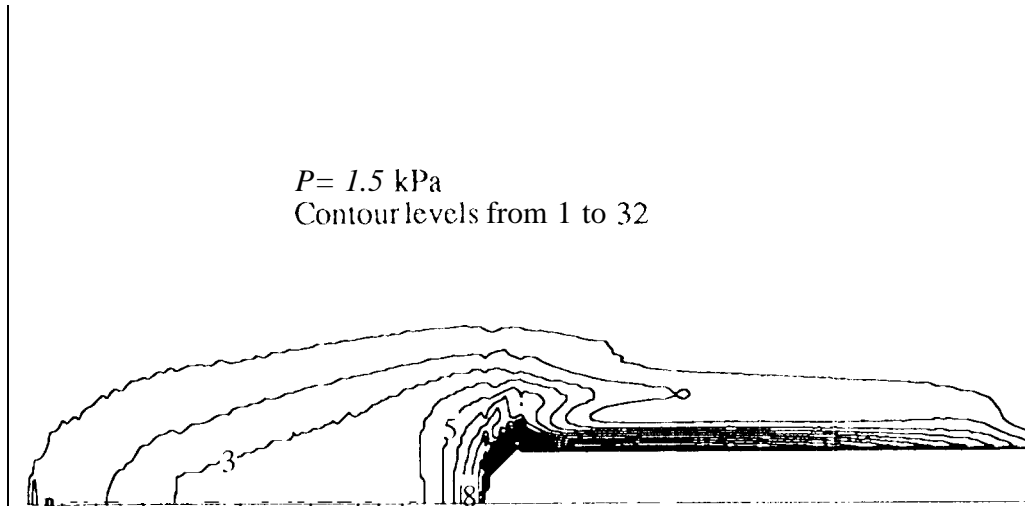


Figure 13: Distribution of the 488 nm Ar II line intensity distribution at 1000 A and 15 kPa

is, the intensity increases with radius and then decreases as one moves from the inside to the outside of this current envelope. This effect can be seen most strongly in the higher pressure cases. Further away, the maximum intensity is on the centerline. Also, the intensity profiles are flat in the radial direction near the tip, particularly in the two low pressure cases, indicating that radial gradients are small. If the intensity levels represent number density levels, then the radial number density and temperature profiles would also be expected to be flat in this region. Recall, that the measured electron temperature profiles for the two lower pressure cases were flat (Fig. (7) and Fig. (8)) suggesting that there is a connection between the strengths of the ion lines and the plasma temperature. However, a means of calibrating the brightness levels is needed for any quantitative results.

The extent of the arc attachment zone is an important parameter in the model because it determines what fraction of the boundary is subjected to the arc heat inputs and is used computationally to limit the total current to the desired value. It is, of course, very difficult to measure directly the surface current density or the heat fluxes. By determining where the largest (brightest) concentration of ions is, the size of the attachment area can be estimated. Since the energy source for the ionization region is primarily the product of the sheath voltage and the thermionic emission current density, it is expected the the plasma will have the largest ion number density (and temperature) where the thermionic current density is highest [3,4]. The thermionic current density can vary over a larger range than the sheath voltage, and therefore dominates. A photomicrograph of the cathode tip after operation at 6 kPa and 1000 A is shown in Fig. (17). The different gray bands are a result of different thorium coverage fractions and therefore different work functions. These characteristics are discussed in more detail below. The changes in work function can significantly affect the current density values [9]. Interestingly the inner edge of the high brightness contours, corresponds to the edge of the white area in the figure.

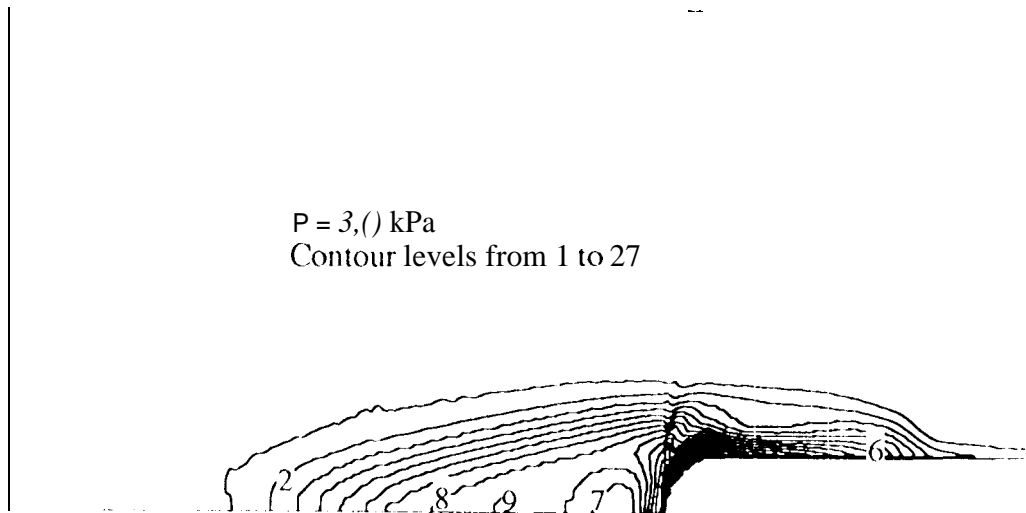


Figure 4: Distribution of the 488 nm Ar II line intensity distribution at 1000 Å and 3.0 kPa

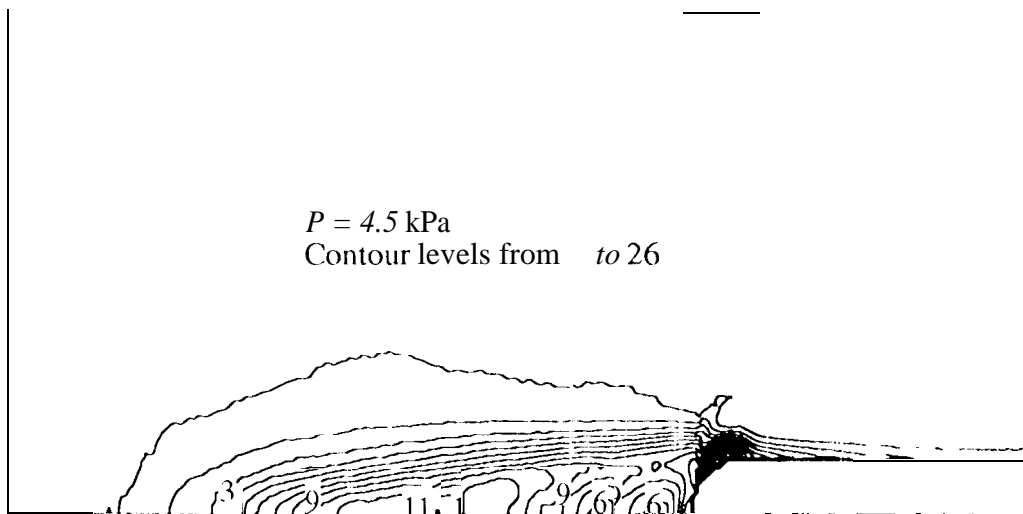


Figure 15: Distribution of the 488 nm Ar II line intensity distribution at 1000 Å and 4.5 kPa

$p = 6.0$ kPa
Contour levels from 1 to 15



Figure 16. Distribution of the 488 nm Ar II line intensity distribution at 1000 A and 6.0 kPa

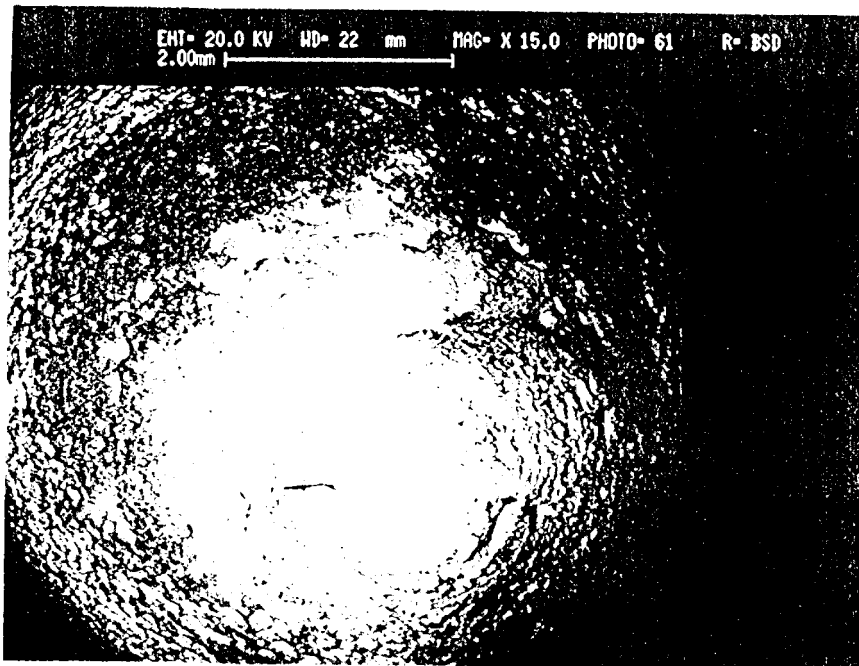


Figure 17. Cathode tip after two hours of operation at 1000 A and 6 kPa

Characterization of the Cathode Surface State

The cathode electron emission capability, and therefore the thermal behavior, is strongly dependent on the surface work function. The surface chemical state and morphology of one of the cathodes used in these experiments were characterized using a scanning electron microscope (SEM) and energy-dispersive spectroscopy (EDS). This cathode had been run for a total of 80 hours at a current level of 1000 A, pressures ranging from 1.5 kPa to 6.0 kPa and argon flow rates of 0.060 to 0.878 g/s. The final two hour run was at a current level of 1000 A, a pressure of 6.0 kPa and a flow rate of 0.276 g/s. Over the course of these tests a shiny protuberance with a diameter of about 2 mm and a height of approximately 1/2 mm developed on the tip of the cathode and a dark band formed around this region. Figure (17) is a photomicrograph of the cathode tip which shows that the tip region can be divided into four zones; the bright white protuberance, the patchy white ring surrounding it, the dark band encircling the white areas and the lighter gray region on the outside. This photograph was taken using backscattered electrons, so the response is sensitive to the elemental composition of the surface. EDS analysis confirmed that the bright white regions are enriched in thorium while the dark areas are essentially pure tungsten. In the central raised area the thorium response was almost as strong as the tungsten response, indicating nearly equal proportions. Higher magnification revealed delicate fern-like structures similar to those found in earlier experiments on the tip of a cathode operated at lower pressures [7]. The ribs of the structures were found to be pure tungsten, while the surrounding areas were pure thorium metal. The patchy region surrounding this was composed of small tungsten crystals and pools of thorium metal. The dark band consisted of the tungsten crystals with no significant traces of thorium, while the outermost region was pure tungsten with a much smoother texture.

The dendritic structures found in the central region are consistent with the existence of a thin molten layer of thorium and tungsten on the tip which solidified at shutdown. The feathery or fern-like structures are formed when the two immiscible components segregate upon cooling. Although the measured tip temperature was only on the order of 2750 K, the phase diagram for this system shows that thorium reduces the freezing point of tungsten to a minimum of 1968 K at the eutectic point^[10]. The tip of the cathode exists in a molten state only because of the high concentration of thorium metal there. The desorption rate of thorium from tungsten at the measured tip temperature greatly exceeds the diffusion rate from the interior, and improbably low gas diffusion rates are required to maintain significant surface coverage [11]. However, the surface structures observed in this zone strongly suggest that thorium vapor condenses on the tip during operation, providing further evidence for a mass transport process first proposed in [7]. At these ambient gas pressures the arc attachment is concentrated on the tip, so an arc column with a high electron density and temperature forms downstream of this region. Evidently metal vapor from the cathode is ionized in the arc column and drawn back to the surface by the electric field. The sheath in these devices is collisionless, so ionization must occur outside the sheath. The weak electric field in the column is apparently sufficient to slow the gas diffusion rate significantly. This also provides a mechanism for mass transport from other regions of the cathode to the region where the arc attaches. Paradoxically, the volatile species accumulate in the hottest zone. The effect is to delay depletion of the thorium at the tip, because it lowers the effective gas diffusion rate and allows access to a much larger supply of thorium. The thorium which can accumulate on the tip is not limited to that available locally; thorium that evaporates from any part of the cathode can conceivably be deposited on the tip if it is first convected into the arc column downstream of the tip.

The tungsten crystals in the dark band were probably formed in a similar process. Tungsten evaporated from the cathode is ionized in the arc column and drawn back to the surface, creating small crystals by vapor deposition. The patchy region between the thorium-rich central area and the ring of tungsten crystals represents a transition zone in which tungsten and thorium vapor are deposited on the surface, but the concentration of thorium is not sufficiently high to lower the melting temperature below the tip temperature. The thorium pools appeared to have been molten during operation, but the tungsten crystals in this region clearly were not. Because there is a surface concentration gradient, thorium may also be supplied to the

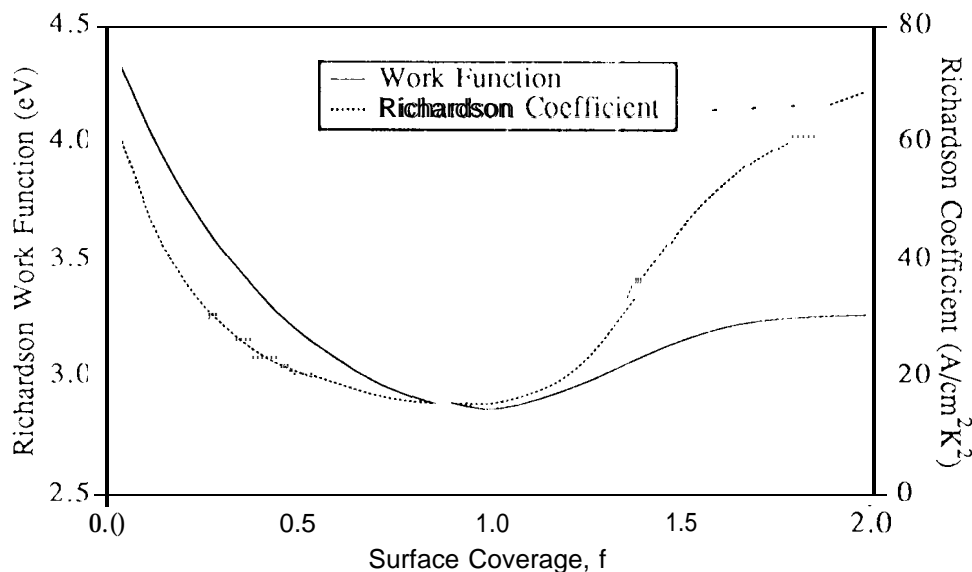


Figure 18: Work function variation of thoriated tungsten.

transition zone from the central region by surface diffusion. The outermost region is evidently a high temperature zone with little vapor deposition of tungsten or thorium. The craters formed during startup have been smoothed out by thermal recrystallization over the course of the final two hour run.

These observations are consistent with cathode surface structures observed at lower pressures and higher discharge currents [7, 11], suggesting that this is representative of cathode operation. A qualitative description of the work function distribution on the cathode surface can be deduced from these surface structures. The work function and Richardson coefficient for thoriated tungsten is dependent on the surface coverage of thorium, as shown in Fig. (18) [17, 2]. The coverage f is defined by N/N_{min} , where N is the number density of adsorbed thorium atoms and N_{min} represents the number density at the minimum work function. The work function is 4.5 eV for pure tungsten, reaches a minimum of approximately 2.8 eV at a thorium coverage of about one half of a complete monolayer and then rises to 3.27 eV, which is about equal to the value for bulk thorium. The surface analysis indicates that this entire range of work functions exists on the cathode during operation. The central region where thorium metal accumulates is probably characterized by a work function close to that of bulk thorium, while the outermost region of pure tungsten would have the highest work function. The intermediate zone represents a transition between these two extremes. The minimum work function and the peak current density therefore occur not on the cathode centerline, but at an intermediate radius on the hemispherical tip. As shown above, this conclusion is consistent with measurements of the argon ion line intensity distribution on the tip.

Model Predictions

A comparison between the quasi-two-dimensional combined plasma and thermal model and the experimental data is shown in Table (1). For the experimental data, the attachment area was estimated from the ion brightness contour plots. The model analysis was performed as follows. The measured tip temperature

was input, and the work function, ϕ , was varied until the calculated attachment area was close to the experimental value. The sheath voltage and the electron temperature were fixed for these inputs. For the 1.5 kPa case, model convergence problems limited how small the area could be made. At this temperature, 5 percent of the particles are singly-charged ions and 29 percent are doubly-charged ions. The convergence problems are a result of the increasing number of triply-charged ions, which are included in the equilibrium portion of the model but not in the other parts. The improvements of the model to include doubly-charged ions is described in Ref. [4]. There appears to be good agreement between the model and the experimental data.

Pressure (kPa)	Experimental Data		Model Parameters					
	Arc Voltage	T_{tip} (K)	Area (cm^2)	T_e (eV)	Area ($(eV)^2$)	V_c	T_e (eV)	ϕ (eV)
1.5	18.3	2527	0.88	1.93	0.88	8.83	1.93	2.93
3.0	17.8	2620	0.58	1.71	0.56	7.54	1.71	2.96
4.5	21.9	2710	0.45	1.62	0.45	6.87	1.62	3.02
6.0	21.6	2750	0.37	1.42	0.37	6.20	1.42	3.04

Table 1 Experimental data and model parameters used in the comparison.

The electron temperature for both arc close, and the calculated sheath voltages are reasonable. The work function for all of the cases are close and in the range of what would be expected. The work function on the tip changes from about 3.27 eV on the center to 4.5 eV far from the tip. It is expected that the transition in thorium coverage would include the minimum in work function described above. It is likely that this is where the attachment area is located. The experimental work function values represent an average value, since the actual surface will have work functions over the entire range.

Model predictions for the plasma parameters for the range of experimental data presented are shown in Figs. (19) through (24). The exponential decrease in attachment area in Figs. (19) and (22) indicates that the majority of the current is from thermionic emission. As the cathode temperature increases (and therefore the thermionic current increases) more energy is added to the ionization region and the electron temperature increases (all other parameters kept constant).

Conclusions

A number of experimental measurements have been made to validate a combined plasma and thermal model that is being developed and to provide values of the input parameters [4]. A database of axial temperature distributions on a cylindrical, 2 percent thoriated tungsten cathode has been collected for a current level of 1000 A for argon mass flow rates of 0.060 to 0.878 g/s and ambient gas pressures ranging from 1.5 to 6.0 kPa. A number of tests were performed to determine what effect mass flow rate has on the axial cathode temperature distribution. No significant effect of the mass flow rate on the axial cathode temperatures was found. If any effect is present, it has been masked by other effects. Electron temperature measurements in the plume downstream of the cathode tip were made using the method of relative line intensity ratios. The radial temperature profiles are flat for the low pressure case and increase radially for the high pressure cases. In general the temperatures decreased approximately exponentially with axial distance from the cathode tip. However, for the high pressure cases, the temperature began to increase downstream indicating that a temperature "depression" exists. The variation of the attachment area with current and pressure was characterized by measuring the intensity distribution of an argon ion line near the cathode surface. For all of the pressures considered the arc is attached in an annular ring around the cathode tip and not on the centerline. Materials analysis of the cathode following a test at 1000 A and 6.0 kPa for two hours revealed that the thorium tends to accumulate at the tip, is depleted on the shaft, and a transition occurs in between. A minimum in the work function therefore occurs in an annulus around the cathode tip.

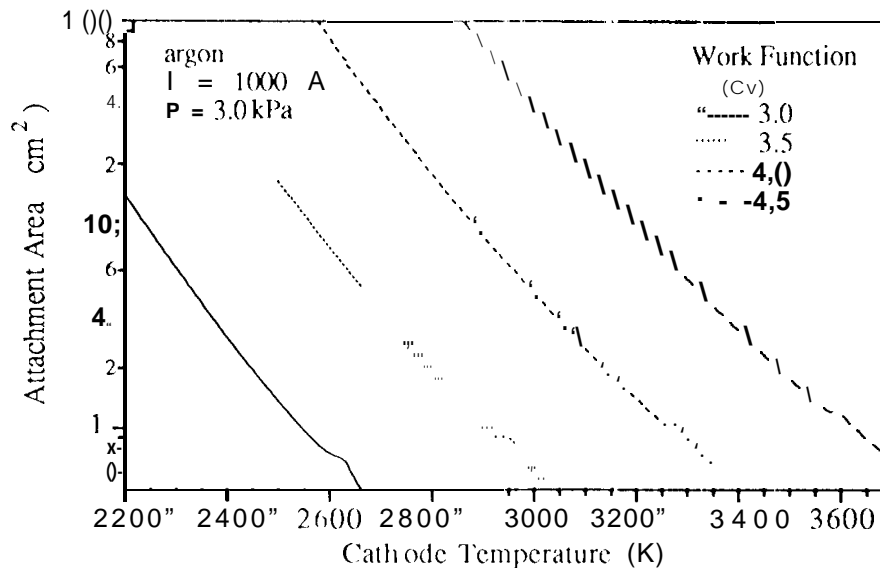


Figure 19: Attachment area as a function of cathode temperature with work function as a parameter.

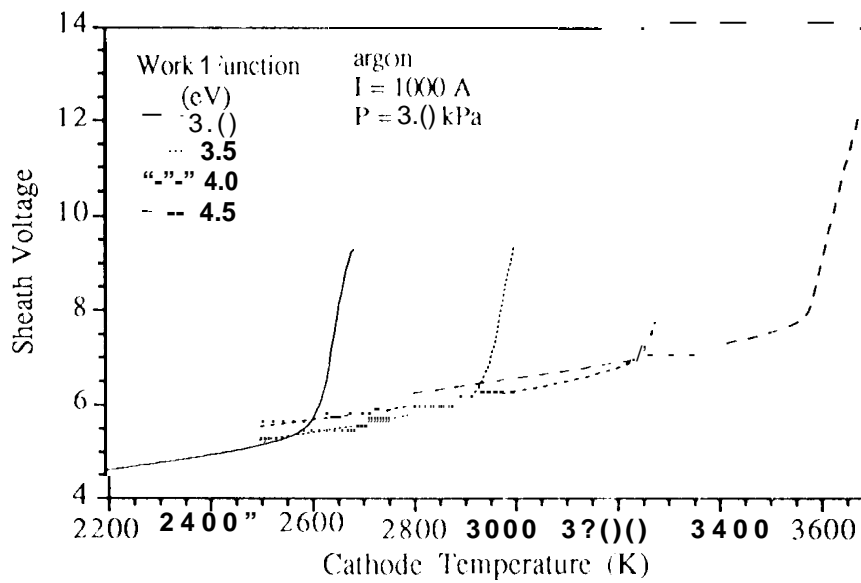


Figure 20: Sheath Voltage as a function of cathode temperature with work function as a parameter.

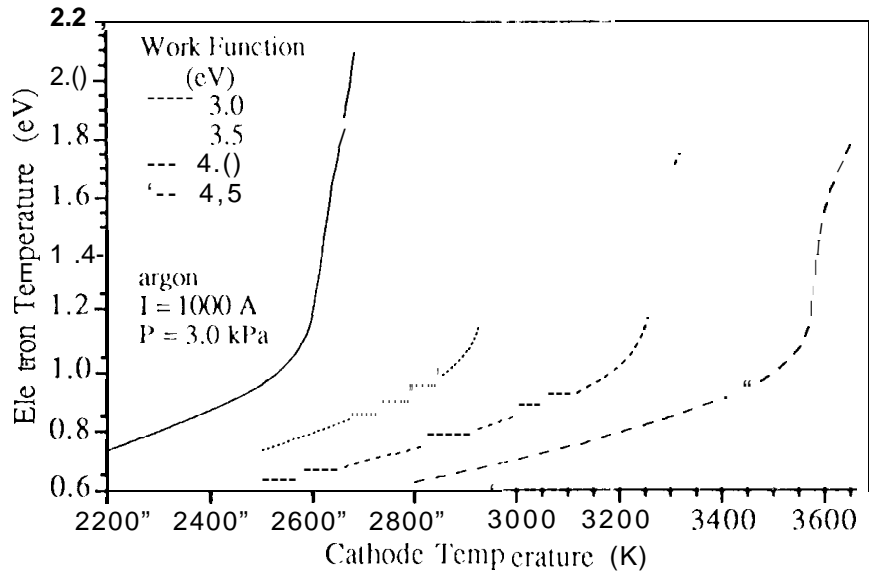


Figure 21: Electron Temperature as a function of cathode temperature with work function as a parameter

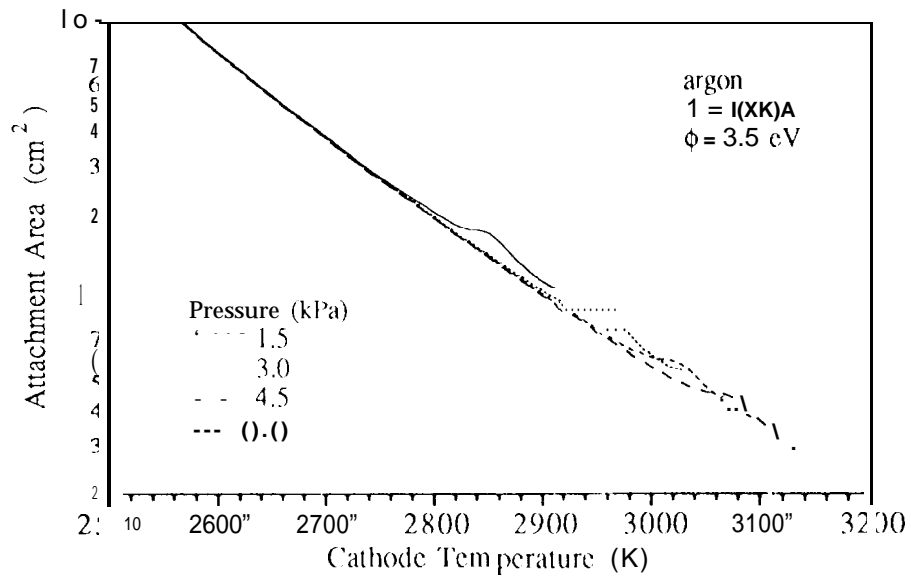


Figure 22: Attachment area as a function of cathode temperature with pressure as a parameter

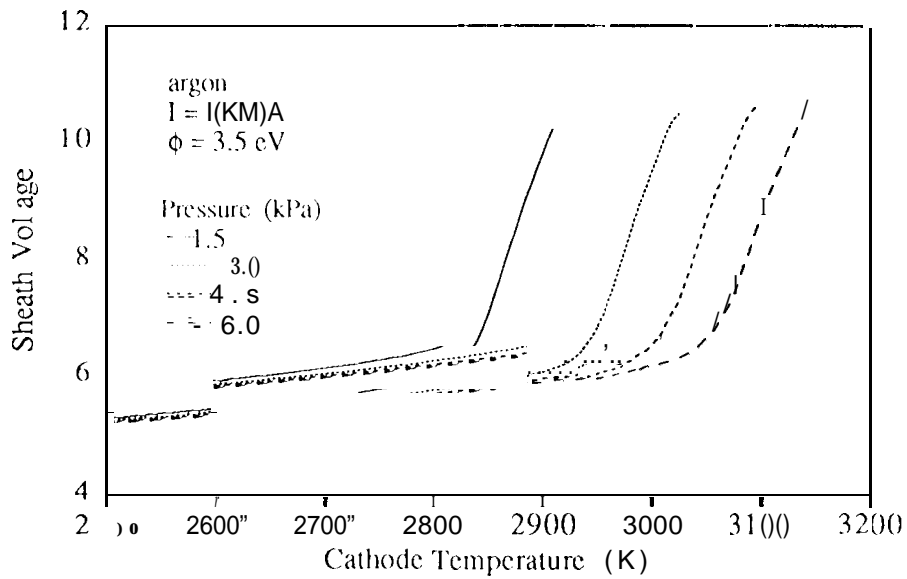


Figure 23: Sheath Voltage as a function of cathode temperature with pressure as a parameter

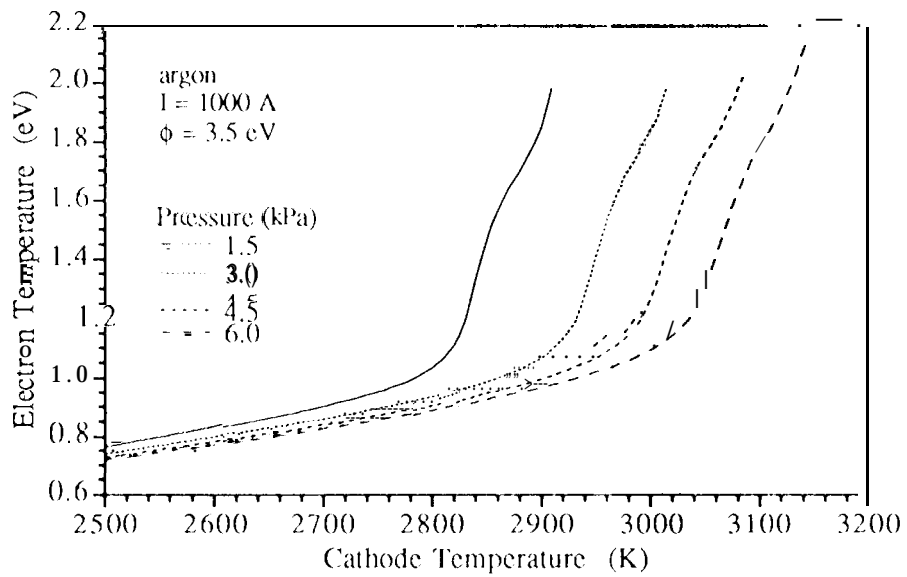


Figure 24: Electron Temperature as a function of cathode temperature with pressure as a parameter.

It is suspected that the current attachment annulus occurs where this minimum in work function is located. Model comparisons with the data show excellent agreement for all of the parameters. The model predicts an average work function of about 3.0 eV for all of the pressures tested. The materials analysis suggests that it should be between 3.27 eV (bulk thorium) and the minimum at 2.8 eV since the attachment area occurs on the edge of the cathode tip.

Acknowledgements

The research described in this paper was conducted at the Jet Propulsion Laboratory, California Institute of Technology, under a contract with the National Aeronautics and Space Administration.

The authors would like to thank W.R. Thogmartin, R.L. Toomath and A.G. Owens for their technical assistance and dedication in constructing the cathode test facility. The assistance of T. J. Pivirotto in setting up the spectrometer and the assistance of Mike Smith in performing the experiments is gratefully acknowledged.

References

- [1] J. E. Polk, A. J. Kelly, and R. G. Jahn. Mechanisms of Hot Cathode Erosion in MPD Thrusters. In *21st International Electric Propulsion Conference*, Orlando, FL, 1990. AIAA-90-2673.
- [2] K. D. Goodfellow and J. E. Polk. High Current Cathode Thermal Behavior, Part I: Theory. In *23rd International Electric Propulsion Conference*, Seattle, WA, 1993. IEPC 93-030.
- [3] K. D. Goodfellow and J. E. Polk. Theoretical Operation of Solid Rod Cathodes. In *30th Joint Propulsion Conference*, Indianapolis, IN, 1994. AIAA 94-3132.
- [4] K. D. Goodfellow. Theoretical Investigation of Cathode Operation in High-Power Ammonia Arcjets. In *31th Joint Propulsion Conference*, San Diego, CA, 1995. AIAA 95-3061.
- [5] J. E. Polk and K. D. Goodfellow. High Current Cathode Thermal Behavior, Part II: Experiments. In *23rd International Electric Propulsion Conference*, Seattle, WA, 1993. IEPC 93-029.
- [6] S.I.Sudharsana. The Abel Inversion of Noisy Data Using Discrete Integral Transforms. MS Thesis, The University of Tennessee, Knoxville, Knoxville, TN, USA, 1986.
- [7] J. E. Polk and K. D. Goodfellow. Experimental Investigation of Solid Rod Cathode Operation In *30th Joint Propulsion Conference*, Indianapolis, IN, 1994. AIAA 94-3131.
- [8] T. M. Randolph, W. F. Von Jaskowsky, A. J. Kelly, and R. G. Jahn. Measurement of Ionization Levels in the Interelectrode region of an MPD Thruster. In *28th Joint Propulsion Conference*, Nashville, TN, 1992. AIAA 92-3460.
- [9] K. D. Goodfellow, T. J. Pivirotto, and J. E. Polk. Applied-Field Magnetoplasma Engine Developments. In *28th Joint Propulsion Conference*, Nashville, TN, 1992. AIAA 92-3293.
- [10] S. Pandian, S.V. Nagender Naidu, and P. Rama Rao. Thorium-tungsten. In T.B. Massalski, editor, *Binary Alloy Phase Diagrams*, volume 3. ASM International, 1990.
- [11] J.E.Polk. *Mechanisms of Cathode Erosion in Plasma Thrusters*. PhD thesis, Princeton University, Princeton, NJ, USA, to be published.
- [12] W. H. Brattain and J. A. Becker. Thermionic and Adsorption Characteristics of Thorium on Tungsten. *Physical Review*, 43:428-450, 1933.